Surface Science and Technology

ORIGINAL ARTICLE Open Access

# Dual impact of $Nd^{3+}$ doping on $CeO_2$ abrasives: enhancing chemical and mechanical effects in chemical–mechanical polishing

Yesheng Zhang[1,2], Hong Lei[1,2*], Jianhua Zhang[2] and Liqiang Luo[1]

**Abstract**

As the demand for advanced optical glass technology increases, improving polishing slurries to enhance material removal rate and reduce surface roughness has become a priority. Cerium oxide is the most widely used abrasive for glass polishing, and its polishing rate is regarded to increase as the surface $Ce^{3+}$ content rises. To improve this, $Nd^{3+}$-doped cerium oxide was prepared using a molten salt method. Morphological and X-ray photoelectron spectroscopy (XPS) analyses showed that the $Nd^{3+}$ doping increased $Ce^{3+}$ content and transformed the particles into an octahedral structure. Additionally, $Nd^{3+}$ doping enhanced the mechanical action, as evidenced by an increased friction coefficient and reduced contact angle. When the doping amount is 4%, $Ce^{3+}$ content and material removal rate peaked at 47.87 nm/min, while the doping amount is 8%, mechanical and chemical synergy achieved the lowest surface roughness of 1.38 nm.

**Keywords** Chemical mechanical polishing, $CeO_2$, Doping, Glass substrate

## 1 Introdution

Chemical mechanical polishing (CMP) technology's development stems from the need for higher surface flatness and smoothness in shrinking semiconductor sizes, smooth transitions between layers in multilayer integrated circuits, and the removal of defects and contaminants to meet stringent surface quality requirements. As integrated circuit sizes shrink, achieving precise planarization becomes essential to reduce defects and optimize the performance of the devices. CMP enables the production of smaller, more complex devices with higher packing densities and improved functionality. These factors collectively drive the advancement of CMP technology in semiconductor manufacturing [1–3]. CMP is a sophisticated technique that achieves precise surface flatness by concurrently considering local and global material aspects [4]. The process combines mechanical abrasion and chemical reactions, with the polishing slurry playing a critical role in influencing material removal rates, surface finishes, and preventing damage to delicate semiconductor structures. The polishing slurry playing a key role in influencing performance and efficiency [5]. The continued advancement of CMP technology is crucial for ensuring the performance and reliability of semiconductor devices, contributing to the development of more powerful and energy-efficient devices.

In these slurries, abrasives exert both mechanical and chemical effects on the workpiece, thereby directly influencing the outcomes of the CMP process [5–7]. $CeO_2$ has moderate hardness and good mechanical action, while it has chemical tooth effect and significant chemical activity [8],which make it widely suitable for chemical mechanical polishing in various products including optical glass [9]. Cerium's ability to exist in various valence

*Correspondence:
Hong Lei
hong_lei2005@163.com
[1] Research Center of Nano Science and Technology, College of Sciences, Shanghai University, Shanghai 200444, China
[2] Shanghai Engineering Research Center for Integrated Circuits and Advanced Display Materials, Shanghai University, Shanghai 200444, China

states and readily switch between them facilitates complexing of $SiO_2$, solidifying $CeO_2$ as an effective polishing abrasives [10]. Sabia and Stevens discovered that during the polishing process, both $Ce^{4+}$ and $Ce^{3+}$ were present on the surface of $CeO_2$ abrasive particles [11]. Xu et al. demonstrated that enhancing the ratio of $Ce^{3+}$ could improve the $CeO_2$ abrasives' polishing efficiency [12]. Schmidt et al. found that trivalent ion doping enhances $Ce^{3+}$ formation on $CeO_2$ crystals [13]. Similarly, Patil et al. found that trivalent ion doping creates many oxygen vacancies in $CeO_2$ without altering its structure [14]. Cheng et al. experimented with lanthanide doping (La, Nd, Yb) on commercial $CeO_2$ abrasives, resulting in a notable enhancement in the abrasives' polishing efficiency on $SiO_2$ matrices [15]. Jin et al. reported a significant increase in the polishing efficiency of $CeO_2$ abrasives with high $Nd^{3+}$ doping, showing a 3.62-fold higher rate compared to pure $CeO_2$ [16]. These studies have confirmed the potential of $Nd^{3+}$ doping to enhance MRR.

However, Cheng and Jin et al. utilized surface immersion and hydrothermal methods for doping, which are commonly used in the synthesis of $CeO_2$. While the salt melting method has been applied in various contexts, its specific advantages for $CeO_2$ synthesis were further demonstrated by Xia's research [17], which showed that $CeO_2$ prepared using the crucible-based salt melting method exhibited a higher $Ce^{3+}$ concentration. The salt melting method has gained significant attention for its environmentally friendly nature, cost-effectiveness, simplicity, and scalability in producing nanomaterials with diverse chemical compositions and morphologies. This technique employs molten salts as a reaction medium to facilitate the dissolution and recrystallization of precursors at elevated temperatures, allowing precise control over particle size and morphology under moderate reaction conditions. In the case of $CeO_2$ synthesis, salt melting method offers distinct advantages over the hydrothermal method. Unlike the latter, salt melting method operates at lower internal pressures during the reaction, reducing the likelihood of $Ce^{3+}$ oxidation by oxygen and water vapor. This results in a higher surface concentration of $Ce^{3+}$, a factor that significantly enhances the material's properties and contributes to improved MRR, as confirmed by Xia's findings. Additionally, Ma et al. investigated $Y^{3+}$, $La^{3+}$, and $Pr^{3+}$ doping of $CeO_2$ by the salt melting method and found that $Y^{3+}$ doped $CeO_2$ exhibited the highest $Ce^{3+}$ concentration and MRR [18]. Furthermore, Xu et al. enhanced MRR by preparing $Y^{3+}$ doped $Ce_{1-x}Y_xO_2$ particles and polishing quartz glass under photocatalysis [19]. These studies have conducted extensive research on the synthesis of cerium oxide and provided a detailed explanation of its chemical mechanisms. However, chemical mechanical polishing involves not only chemical interactions but also significant mechanical actions and the wetting effects of the polishing slurry. These aspects were not addressed in the previous research by Ma and Xu et al. Specifically, their conclusions regarding the mechanical actions lack a solid theoretical foundation. Therefore, further testing of its mechanical properties is required.

In this work, the abrasives $Ce_{1-x}Nd_xO_2$ with different doping amounts were synthesized using the molten salt method (x is the doping amount of $Nd^{3+}$ in $CeO_2$, x = 0.00, 0.02, 0.04, 0.06, 0.08, 0.10). The chemical and mechanical effects of CMP were investigated, and a mechanism for CMP was proposed.

## 2 Experimental and methods

### 2.1 Preparation of $Ce_{1-x}Nd_xO_2$ abrasives

The abrasives $Ce_{1-x}Nd_xO_2$ with different doping amounts were synthesized using the molten salt method [18] (x is the doping amount of $Nd^{3+}$ in $CeO_2$, x = 0.00, 0.02, 0.04, 0.06, 0.08, 0.10). However, it is worth noting that the reaction temperature was optimized (800° C) to ensure that the particle size remained in a suitable range.

### 2.2 Characterization of the abrasives and polishing slurry

The descriptions of the characterization details are reported in the supporting information (S1).

### 2.3 CMP experiment

The preparation method for the CMP polishing slurry is as follows: adding the abrasive to deionized water (PH = 10), dispersing it with ultrasonic waves for 10 min, stirring with a magnetic agitator for 5 min, and then conducting the CMP test. The experimental details are shown in Table 1.

After polishing, MRR is calculated by Eq. (1) [18, 20]:

**Table 1** Polishing process details

| Parameter | Specification |
|---|---|
| Polishing machine | UNIPOL-1000S, Shenyang Kejing Instrument Co., LTD., China |
| Polishing time | 3 min |
| Polishing load | 3.5 kg |
| Platen's rotation speed | 80 r/min |
| Carrier's rotation speed | 80 r/min |
| Polishing slurry: Solid content | $Ce_{1-x}Nd_xO_2$ abrasive 1.5 g (0.5wt %) |
| Polishing slurry: Solvent content | deionized water 300 ml (PH = 10) |
| Polished substrate | pristine soda lime glass (diameter 50 mm) |
| polishing pad | Rodel porous polyurethane pad |

$$MMR = \frac{\Delta m^* 10^4}{\rho \pi R^2 \tau} \quad (1)$$

MRR: Material removal rate (nm/min); Δ m: The material mass (g) removed from the glass substrate during polishing, obtained by calculating the quality difference of the glass substrate before and after polishing. The quality of the glass substrate before and after polishing was obtained by acetone cleaning and drying and weighing. R: substrate radius (cm); τ: Polishing time (min); ρ: Density of substrate ($\rho_{glass}$ = 2.5 g /cm3).

## 3 Results and discussions

### 3.1 Phase and morphology analysis

The XRD pattern of $Ce_{0.9}Nd_{0.1}O_2$ abrasive and $CeO_2$ abrasive are shown in Fig. 1. The diffraction peaks of $CeO_2$ are located at 2θ values of approximately 28.6°, 33.2°, 47.6°, 56.4°, 59.2°, 69.5°, 76.7°, and 79.1°. These peaks correspond to the (111), (200), (220), (311), (222), (400), (331), and (420) planes of the $CeO_2$ phase, as referenced in PDF#04–002-3313. For $Ce_{0.9}Nd_{0.1}O_2$, the diffraction peaks are observed at 2θ values around 28.5°, 33.1°, 47.5°, 56.3°, 59.1°, 69.4°, 76.7°, and 79.1°, which are also associated with the (111), (200), (220), (311), (222), (400), (331), and (420) planes of the $CeO_2$ phase, according to the same reference. Comparing the diffraction peaks of $Ce_{0.9}Nd_{0.1}O_2$ with $CeO_2$, it is evident that $Nd^{3+}$ doping does not notably shift the overall peak positions of cerium oxide, confirming that it remains in the cerium oxide phase without the appearance of impurity peaks related to Nd, thus confirming the successful doping. In the XRD pattern of $Ce_{0.9}Nd_{0.1}O_2$, the larger radius of $Nd^{3+}$ (99.5 pm) compared to $Ce^{4+}$ (92 pm) [21] causes lattice expansion in $CeO_2$, resulting in a peak shift [18] towards lower angles.

The shape and size of abrasives significantly impact the mechanical effectiveness in CMP processes. Figure 2(a)-(f) displays SEM images of $CeO_2$ abrasive and $Ce_{1-x}Nd_xO_2$ abrasives. As shown in Fig. 2(a), the $CeO_2$ abrasive particles have a polyhedral shape with an average size of 534 nm. In contrast, Fig. 2(b)-(g) illustrate that the particle size of $Ce_{1-x}Nd_xO_2$ abrasive is all smaller than $CeO_2$, and the particle size decreases with increasing of $Nd^{3+}$ doping levels. As the particle size decreases, the depth to which the abrasive penetrates the substrate material during the polishing process is reduced, leading to a decrease in the mechanical action. Alternatively, the shape of $Ce_{1-x}Nd_xO_2$ abrasives transitions from polyhedral to octahedral as the $Nd^{3+}$ doping increases, maintaining a primarily octahedral structure when the doping level reaches 4%. The octahedral shape, with its sharper edges compared to those of polyhedral shapes, generates greater point pressure during the polishing process, thereby increasing the material removal rate from the substrate. Figure 3 (a)-(b) shows the EDS spectra of $CeO_2$ abrasive and $Ce_{0.9}Nd_{0.1}O_2$ abrasive. Only Ce and O elements exist in the EDS results of $CeO_2$ abrasive, while Ce, O and Nd elements exist in $Ce_{0.9}Nd_{0.1}O_2$ abrasives, which also confirms the success of $Nd^{3+}$ doping [18].

The zeta potential method measures system stability [22], a higher absolute zeta potential implies increased repulsive forces between particles, leading to greater

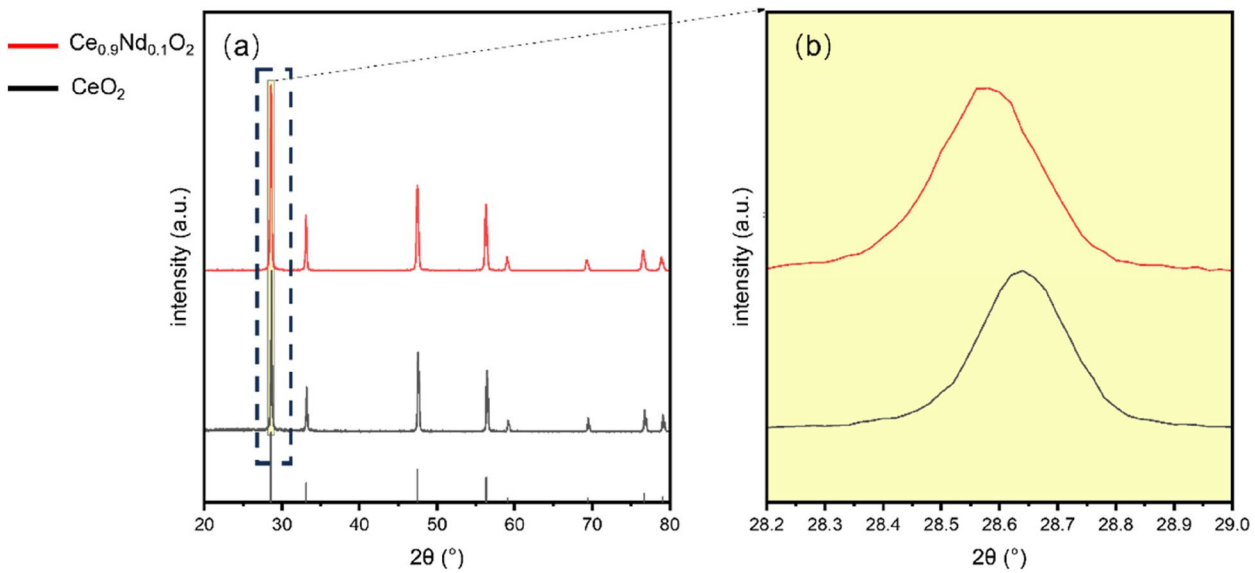


**Fig. 1** **a** XRD pattern of prepared $CeO_2$ and $Ce_{0.9}Nd_{0.1}O_2$ (compared with $CeO_2$ standard PDF cards, **b** Partially enlarged view of the XRD pattern shown in (**a**)

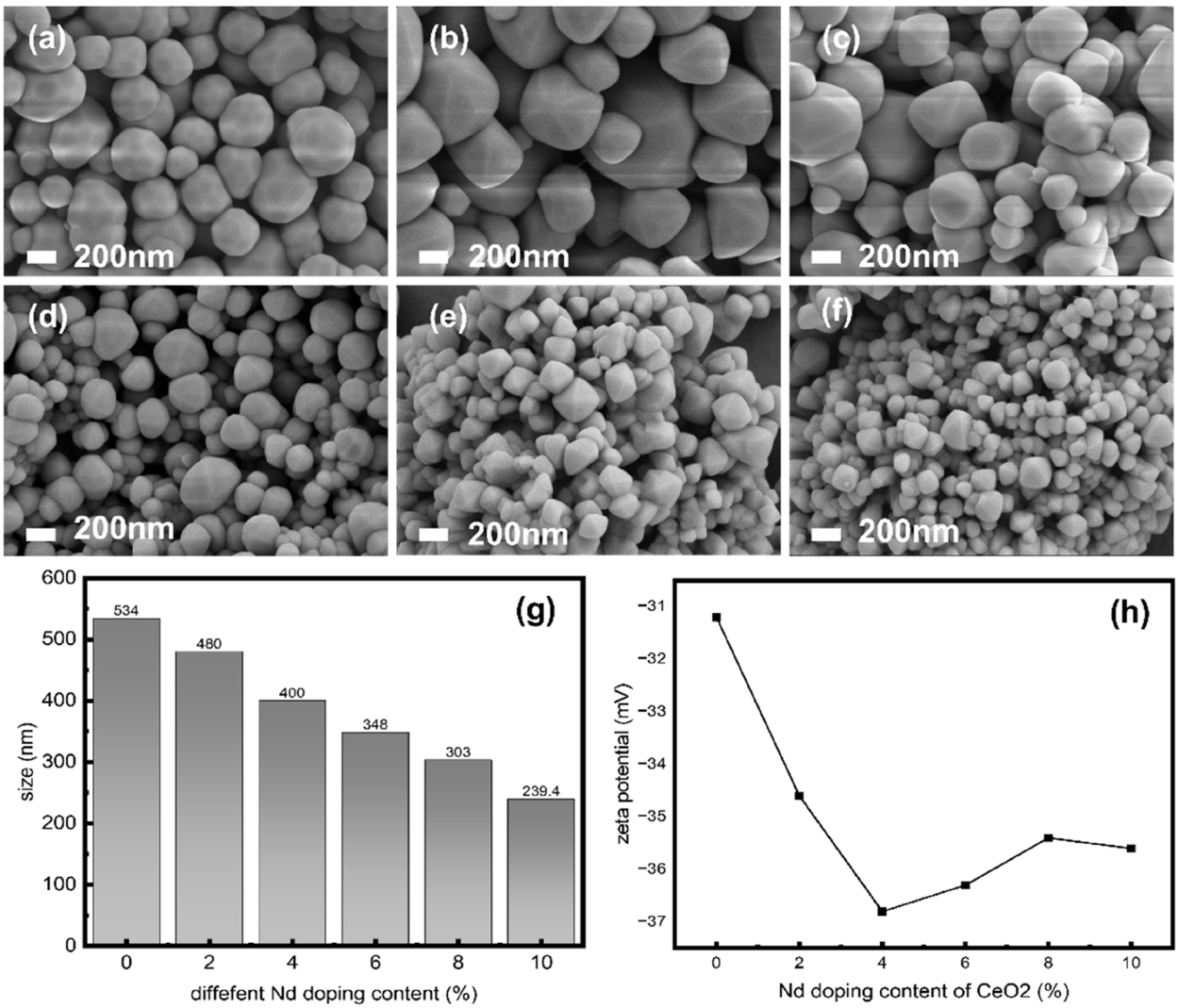


**Fig. 2** SEM images of $Ce_{1-x}Nd_xO_2$ abrasives (x is the content of $Nd^{3+}$ doping in $CeO_2$, x = (**a**) 0%, (**b**) 2%, (**c**) 4%, (d)6%, (**e**) 8%, (f)10%), (**g**) particle size of $Ce_{1-x}Nd_xO_2$ abrasives and (h)zeta potential of $Ce_{1-x}Nd_xO_2$ polishing slurry

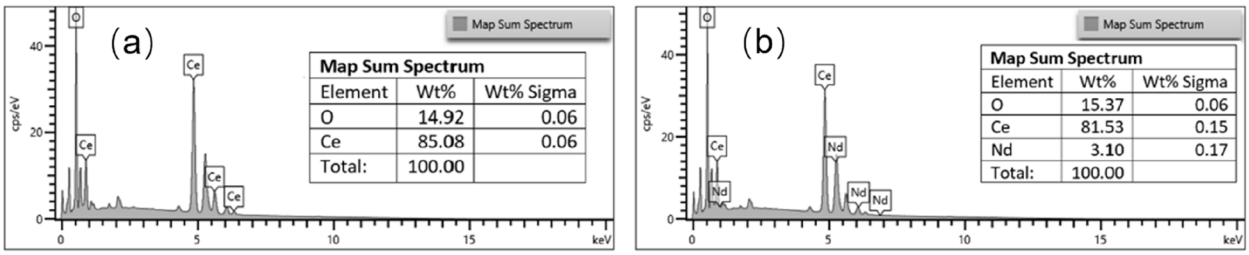


**Fig. 3** EDS spectra of (**a**) pure $CeO_2$ abrasive and (**b**) $Ce_{0.9}Nd_{0.1}O_2$ abrasive

stability. Generally, a zeta potential above 30 mV indicates a more stable suspension [23]. Figure 2(h) shows that the zeta potential of polishing slurry prepared by $CeO_2$ abrasive is -31.2 mV, indicating that the polishing slurry made from $CeO_2$ prepared by this method is relatively stable. Furthermore, the absolute zeta potential of the polishing slurries prepared with doped $Ce_{1-x}Nd_xO_2$ abrasives is higher than $CeO_2$ abrasive. This indicates

that $Nd^{3+}$ doping enhances the stability of $Ce_{1-x}Nd_xO_2$ abrasives polishing slurries. When the doping amount is 4%, the absolute zeta potential is at its highest, suggesting that the polishing slurry exhibits the greatest stability.

### 3.2 Surface defect analysis

Figure 4(a) presents the XPS spectrum of the $CeO_2$ abrasive and $Ce_{1-x}Nd_xO_2$ abrasives. The spectrum for $CeO_2$ abrasive reveals the presence of only Ce and O elements, with no detectable K, Na, Cl, or Nd elements. Conversely, the spectrum for $Ce_{1-x}Nd_xO_2$ abrasives reveals the presence of Ce, Nd, and O elements, but no K, Na, or Cl elements. The absence of detectable K, Na, Cl elements in both the $CeO_2$ abrasive and $Ce_{1-x}Nd_xO_2$ abrasives indicating that no residual salts are present on the surface. Additionally, peaks observed in the $Ce_{1-x}Nd_xO_2$ abrasives spectrum at 982.3 eV and 1005.8 eV correspond to Nd $3d_{3/2}$ and Nd $3d_{5/2}$, respectively. The results confirm $Nd^{3+}$ ions are located at the surface of $Ce_{1-x}Nd_xO_2$ abrasives. Combined with XRD and EDS results, it is evident that $Nd^{3+}$ ions are successfully doped in the $Ce_{1-x}Nd_xO_2$ abrasives.

As $Ce^{3+}$ is a key factor in the polishing process of $CeO_2$ surfaces, The Ce 3d characteristic spectrum is analyzed, with the spin-orbitals $3d_5/_2$ and $3d_3/_2$ represented by the symbols "v" and "u," respectively. The peaks corresponding to $Ce^{3+}$ are marked as $v_0$, v', $u_0$, and u', whereas the peaks for $Ce^{4+}$ are labeled v, v", v"', u, u", and u"' [19]. The final XPS fitting results are shown in Fig. 4(b)-(g), with more detailed peak area data and binding energies provided in Table 2. The $Ce^{3+}$ concentration of $CeO_2$ and $Ce_{1-x}Nd_xO_2$ abrasives was calculated using Eqs. (2)-(4), and the results are shown in Fig. 4(h). The findings indicate that the $Ce^{3+}$ concentration of $CeO_2$ abrasive surface is only 22.51%, while the $Ce^{3+}$ concentration of $Ce_{1-x}Nd_xO_2$ abrasive surface is higher. Specifically, the $Ce_{0.96}Nd_{0.04}O_2$ abrasive surface exhibited the highest $Ce^{3+}$ concentration, at 37.68%.

$$C\left(Ce^{3+}\right) = \frac{A\left(Ce^{3+}\right)}{A\left(Ce^{3+}\right) + A\left(Ce^{4+}\right)} \tag{2}$$

$$A\left(Ce^{3+}\right) = A(V_0) + A\left(V'\right) + A(U_0) + A\left(U'\right) \tag{3}$$

$$A\left(Ce^{4+}\right) = A(V) + A\left(V''\right) + A\left(V'''\right) + A(U) + A\left(U''\right) + A\left(U'''\right) \tag{4}$$

Additionally, the oxygen vacancy content on $CeO_2$ abrasive was found to correlate positively with the $Ce^{3+}$ content. The O 1 s characteristic spectrum was examined, as shown in Fig. 5(a)-(f). The peaks at 529 eV, 531 eV, and 533 eV correspond to lattice oxygen (Oα), surface oxygen (Oβ), and adsorbed oxygen (Oγ), respectively [24]. Here, Oβ represents the oxygen vacancy present in the $CeO_2$ abrasive, which can be calculated by Eq. (5). Calculated oxygen vacancy concentration of the $CeO_2$ and $Ce_{1-x}Nd_xO_2$ abrasive surface are shown in Fig. 5(g). The results show that the oxygen vacancy concentration on the $CeO_2$ abrasive surface is 34.44%, whereas it is higher on the $Ce_{1-x}Nd_xO_2$ abrasive surface. Specifically, the $Ce_{0.96}Nd_{0.04}O_2$ abrasive surface exhibits the highest surface oxygen vacancy concentration (45.20%). This indicates that more $Ce^{4+}$ is reduced to $Ce^{3+}$ in the $Ce_{1-x}Nd_xO_2$ crystal, aligning with the calculated $Ce^{3+}$ concentration.

$$C\left(\text{oxygen vacancy}\right) = O\beta/(O\alpha + O\beta + O\gamma) \tag{5}$$

Furthermore, Raman spectroscopy was employed to further verify the presence of oxygen vacancies on $CeO_2$ abrasives. As depicted in Fig. 6. The peak around 460 $cm^{-1}$ represents the F2g vibration mode of cubic $CeO_2$ [25], while the peak at 600 $cm^{-1}$ indicates doping-related structural defects [21]; the ratio of these peak intensities (I600/I460) reflects the concentration of oxygen vacancies in $CeO_2$ [26],as shown in Eq. (6):

$$C\left(\text{oxygen vacancy}\right) = (1600/1460) \tag{6}$$

The oxygen vacancy concentration is 0.58% for $CeO_2$ abrasives and higher for $Ce_{1-x}Nd_xO_2$ abrasives, with $Ce_{0.96}Nd_{0.04}O_2$ showing the highest at 3.39%. This indicates more $Ce^{4+}$ is reduced to $Ce^{3+}$, consistent with both XPS and Raman spectroscopy results.

### 3.3 Contact angle analysis

The effect of $Nd^{3+}$ doping on the surface hydrophilicity of polishing slurries prepared with $CeO_2$ abrasives and $Ce_{1-x}Nd_xO_2$ abrasives was further investigated. Static contact angles between polishing slurries prepared by $CeO_2$ abrasive and $Ce_{1-x}Nd_xO_2$ abrasives and glass substrates were measured by a contact angle measurement instrument, as shown in Fig. 7. The contact angle between pure water and the glass substrate is 48.3°. However, the contact angle between the polishing slurries and the glass substrate decreases with the addition of $CeO_2$ abrasive and $Ce_{1-x}Nd_xO_2$ abrasives. The minimum contact angle observed was 22.6°, which was obtained with polishing slurries prepared by $Ce_{0.96}Nd_{0.04}O_2$ abrasive. These results indicate that $Nd^{3+}$ doping can improve the hydrophilicity of polishing slurries prepared by $CeO_2$ abrasive and $Ce_{1-x}Nd_xO_2$ abrasives. When the doping amount is 4%, the contact angle reaches its minimum. This matches the XPS results, showing that the higher $Ce^{3+}$ concentration on the $Ce_{1-x}Nd_xO_2$ improves bonding with the $SiO_2$ in the glass substrate. Therefore, it is

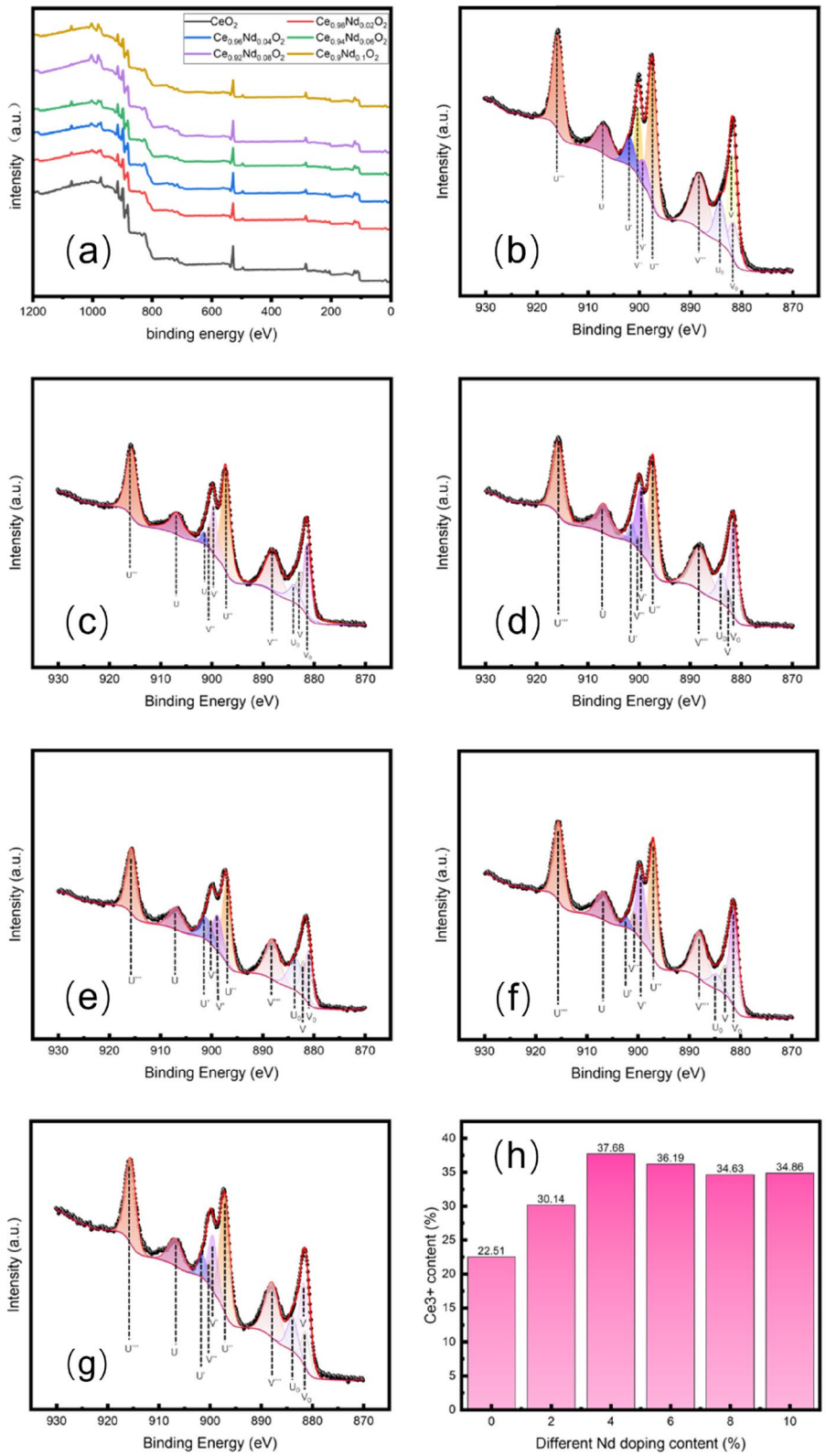


**Fig. 4** XPS spectra of abrasives: (**a**) Survey of $CeO_2$ and $Ce_{1-x}Nd_xO_2$; (**b**-**d**) Ce 3d spectra of $CeO_2$, $Ce_{0.98}Nd_{0.02}O_2$, $Ce_{0.96}Nd_{0.04}O_2$. **e**–**g** Ce 3d spectra of $Ce_{0.94}Nd_{0.06}O_2$, $Ce_{0.92}Nd_{0.08}O_2$, $Ce_{0.}Nd_{0.1}O_2$ respectively; (**h**) $Ce^{3+}$ concentration of the $CeO_2$ and $Ce_{1-x}Nd_xO_2$ abrasive surface

**Table 2** The binding energies and peak areas for the abrasives

| | $Ce^{3+}$ | | | | $Ce^{4+}$ | | | | | | $Ce^{3+}$content |
|---|---|---|---|---|---|---|---|---|---|---|---|
| | $V_0$ | V′ | $U_0$ | U′ | V | V″ | V‴ | U | U″ | U‴ | |
| $CeO_2$ | | | | | | | | | | | |
| BE (eV) | 881.47 | 899.11 | 884.22 | 901.82 | 881.85 | 900.18 | 888.21 | 906.93 | 897.45 | 915.90 | |
| Area | 18720 | 12770 | 21068 | 14372 | 40793 | 22666 | 43956 | 21555 | 55225 | 46152 | 22.51% |
| $Ce_{0.98}Nd_{0.02}O_2$ | | | | | | | | | | | |
| BE (eV) | 881.36 | 899.64 | 883.95 | 901.55 | 882.47 | 900.39 | 888.08 | 906.87 | 897.28 | 915.67 | |
| Area | 25616 | 25390 | 12517 | 3002 | 25898 | 6052 | 27011 | 18609 | 43444 | 34901 | 30.14% |
| $Ce_{0.96}Nd_{0.04}O_2$ | | | | | | | | | | | |
| BE (eV) | 881.44 | 899.55 | 883.72 | 901.32 | 882.58 | 900.18 | 888.00 | 906.90 | 897.21 | 915.77 | |
| Area | 41357 | 33435 | 15434 | 7382 | 5566 | 2257 | 39078 | 28881 | 42239 | 40045 | 37.68% |
| $Ce_{0.94}Nd_{0.06}O_2$ | | | | | | | | | | | |
| BE (eV) | 881.01 | 898.79 | 883.47 | 901.07 | 882.02 | 900.05 | 888.09 | 906.94 | 897.04 | 915.65 | |
| Area | 19485 | 17704 | 22392 | 13932 | 12500 | 8257 | 27638 | 15228 | 32380 | 32418 | 36.19% |
| $Ce_{0.92}Nd_{0.08}O_2$ | | | | | | | | | | | |
| BE (eV) | 881.26 | 899.43 | 884.64 | 902.24 | 882.86 | 900.66 | 887.98 | 906.77 | 897.00 | 915.51 | |
| Area | 41854 | 30720 | 8929 | 3375 | 13569 | 7376 | 32519 | 19135 | 46112 | 39321 | 34.63% |
| $Ce_{0.}Nd_{0.1}O_2$ | | | | | | | | | | | |
| BE (eV) | 881.60 | 899.41 | 883.86 | 901.46 | 881.24 | 900.14 | 887.85 | 906.74 | 897.10 | 915.57 | |
| Area | 29594 | 19009 | 12245 | 7382 | 10427 | 4926 | 27890 | 13728 | 38469 | 30847 | 34.86% |

reflected at the macro level that the polishing slurries exhibits lower contact angle performance. In the CMP process, the contact angle between the slurry and the glass substrate plays a key role in both the chemical and mechanical actions of the polishing process. A smaller contact angle leads to a higher diffusion coefficient of the slurry on the glass surface, increasing the contact area. Consequently, a reduced contact angle allows the effective substances in the slurry to diffuse more efficiently to the glass surface during polishing, enhancing the chemical reaction at the interface and may improving the $SiO_2$ removal rate [27]. Additionally, a smaller contact angle increases the mechanical interaction by enlarging the contact area, thereby enhancing the abrasion effect. Conversely, if the contact angle between the polishing liquid and the glass substrate increases, it would reduce the diffusion of active substances to the wafer surface and decrease the contact area, thereby diminishing both the chemical reaction and the mechanical abrasion efficiency, ultimately may lowering the $SiO_2$ removal rate. This offers a more intuitive understanding of the mechanical behavior of doped cerium oxide polishing slurry.

### 3.4 Friction coefficient

In the CMP process, mechanical action is crucial for material removal. It relies on both chemical reactions and mechanical wear. Greater mechanical forces lead to increased contact pressure, enhancing the abrasive particles' wear effect on the material surface [28]. A higher coefficient of friction results in greater friction under the same normal force. This increased friction enhances the scraping and cutting actions of the abrasive particles on the material surface, thereby improving wear efficiency. Consequently, more material can be removed per unit time. The dynamic friction coefficient (COF) of $CeO_2$ and $Ce_{1-x}Nd_xO_2$ abrasives was measured using a friction coefficient meter. According to Fig. 8, pure $CeO_2$ has the lowest average COF at 0.37. In contrast, the COF of $Ce_{1-x}Nd_xO_2$ abrasives doped with $Nd^{3+}$ is higher. Notably, when the $Nd^{3+}$ doping amount is 4%, the dynamic COF reaches its maximum value of 0.42. This may be due to the improved adhesion between the polishing particles and the $SiO_2$ in the glass substrate. More bonding leads to increased polishing resistance. This is also consistent with XPS and contact angle changes. When the doping amount is 4%, the abrasive particles have the highest surface $Ce^{3+}$ concentration, allowing for better bonding with the $SiO_2$. Simultaneously, the polishing particles achieve greater contact with the glass substrate, facilitating increased bonding between abrasive and the substrate. Consequently, polishing resistance and the COF increase. However, in the previous XPS analysis, with $Nd^{3+}$ doping at 6%, the surface $Ce^{3+}$ content was found to be less than 4%. Interestingly, despite both samples exhibiting an octahedral morphology, the COF remained identical to that of the 4% doping level. The primary distinction lay in the size of the abrasives: 400 nm for the 4% doping and 348 nm for the 6% doping. This observation suggests that

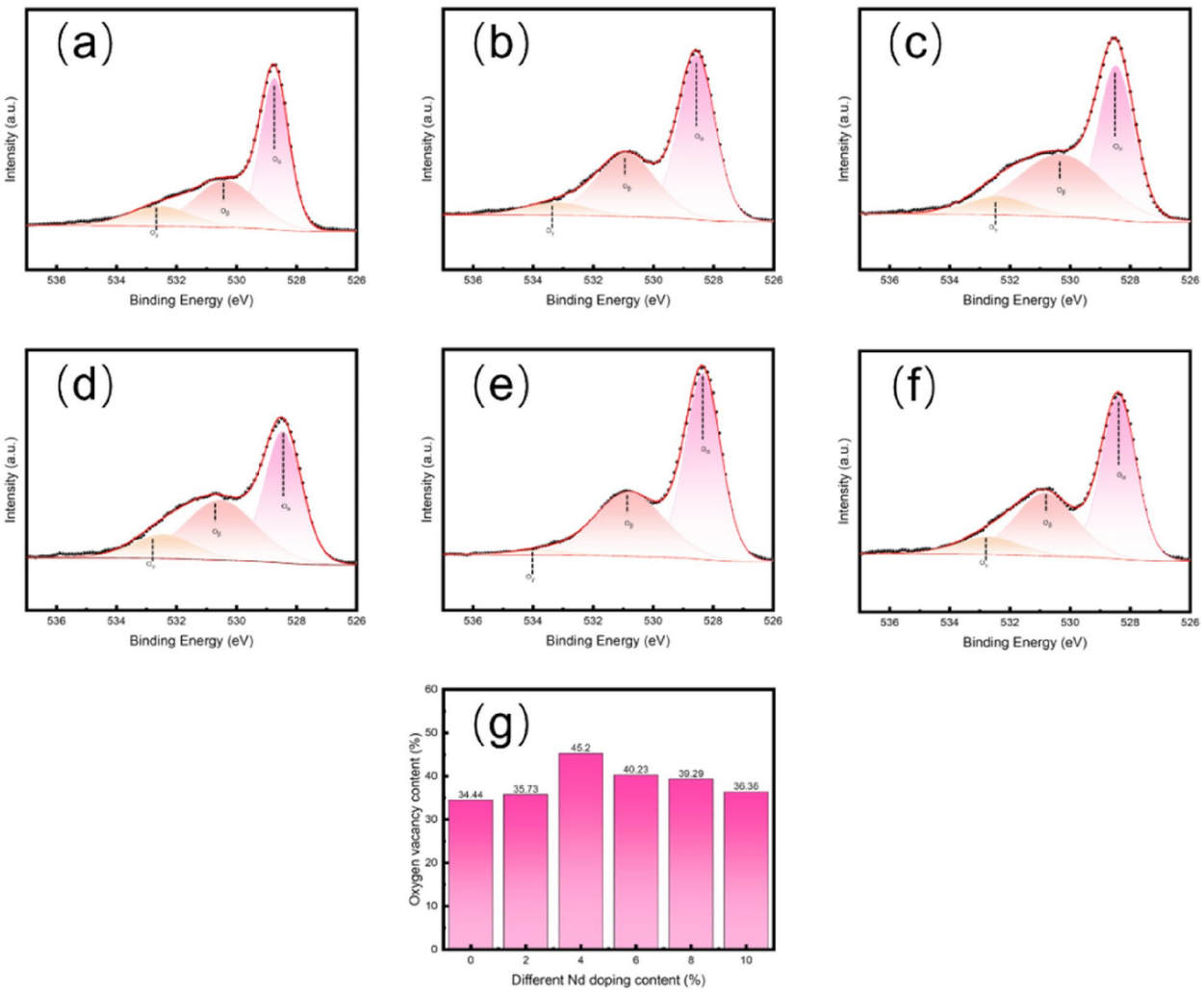


**Fig. 5** XPS spectra of $CeO_2$ abrasives (**a**-**g**) O 1 s spectra of $CeO_2$, $Ce_{0.98}Nd_{0.02}O_2$, $Ce_{0.96}Nd_{0.04}O_2$, $Ce_{0.94}Nd_{0.06}O_2$, $Ce_{0.92}Nd_{0.08}O_2$, $Ce_{0.}Nd_{0.1}O_2$ respectively; (**h**) Oxygen vacancy concentration of the $CeO_2$ and $Ce_{1-x}Nd_xO_2$ abrasive surfaces

at an abrasive size of 348 nm, there is improved contact between the abrasive particles and the glass substrate, which compensates for the lower $Ce^3+$ content and enhances their adhesion. This underscores the critical role of particle size in mechanical interactions.

### 3.5 Material removal rate (MRR) analysis

Improved material removal rates contribute to saving processing time and reducing abrasive costs. Therefore, achieving high material removal rates is a common goal in the industry [29]. Figure 9 shows that the MRR for glass substrates polished with $Ce_{1-x}Nd_xO_2$ abrasives ranges from 35.99 to 47.87 nm/min, significantly higher than the 28.18 nm/min of $CeO_2$ abrasives. $Nd^{3+}$ doping improves polishing efficiency, with $Ce_{0.96}Nd_{0.04}O_2$ showing the highest MRR, 69.88% greater than pure $CeO_2$. This enhancement is due to better bonding between the abrasive and $SiO_2$ and the effective mechanical action of larger, polyhedral particles when doping is under 4%. However, the MRR does not peak due to low chemical activity. At low doping levels, the abrasive's chemical activity is the primary factor affecting MRR. Reduced chemical activity limits bonding between abrasive particles and the glass substrate, resulting in inadequate $SiO_2$ removal and a lower MRR.

When the doping amount is 4%, the $Ce^{3+}$ concentration on the surface of the abrasive reaches its highest level, resulting in the strongest chemical interaction during the polishing process. This enhances the formation of chemical bonds between the abrasive particles and $SiO_2$, allowing for more efficient removal of $SiO_2$ fragments from the substrate material. At this doping level, the morphology of the abrasives transitions to an octahedral shape, which further enhances the mechanical action during polishing.

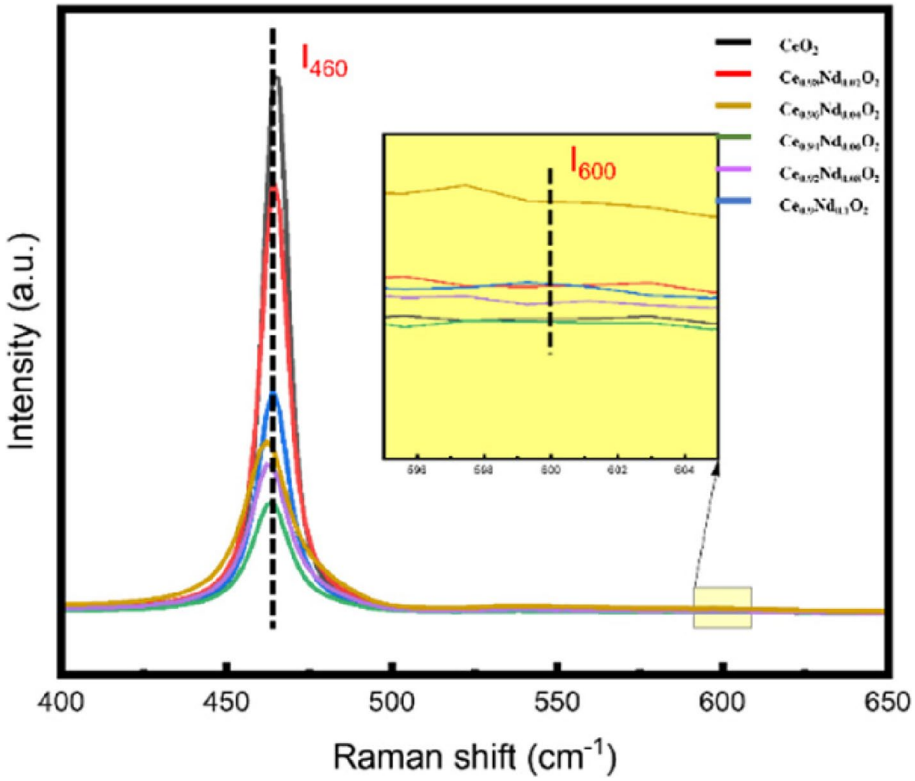


**Fig. 6** Raman spectra of $CeO_2$ and $Ce_{1-x}Nd_xO_2$

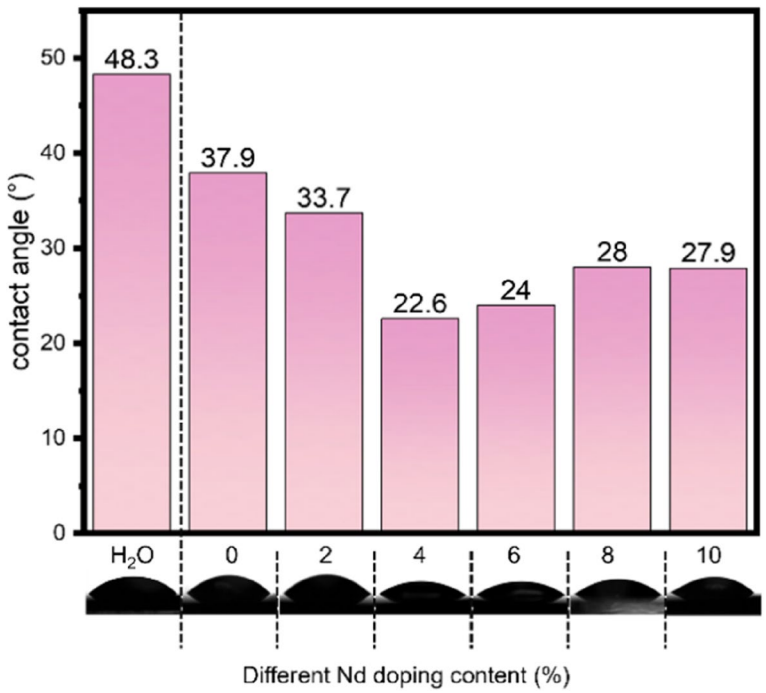


**Fig. 7** The contact angle of $CeO_2$ and $Ce_{1-x}Nd_xO_2$ slurries on glass substrate

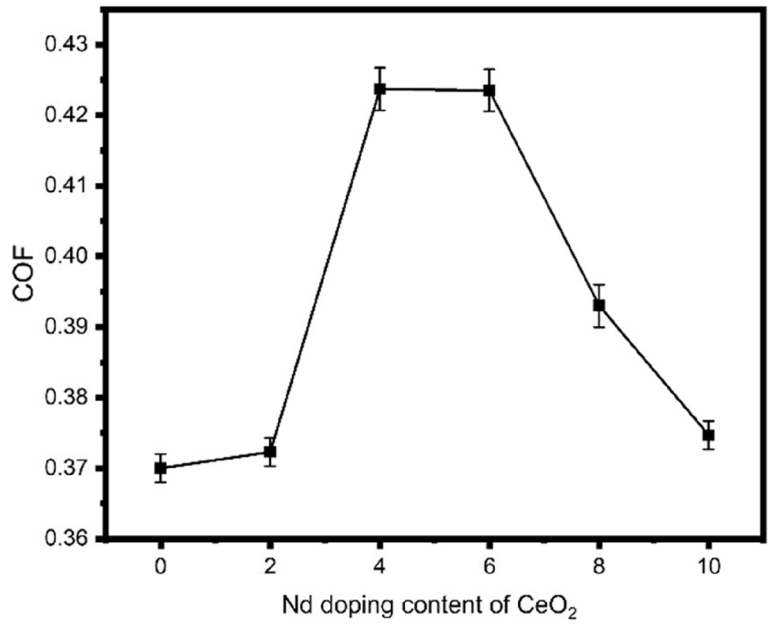


**Fig. 8** Coefficient of friction vs. different $Nd^{3+}$ doping contents

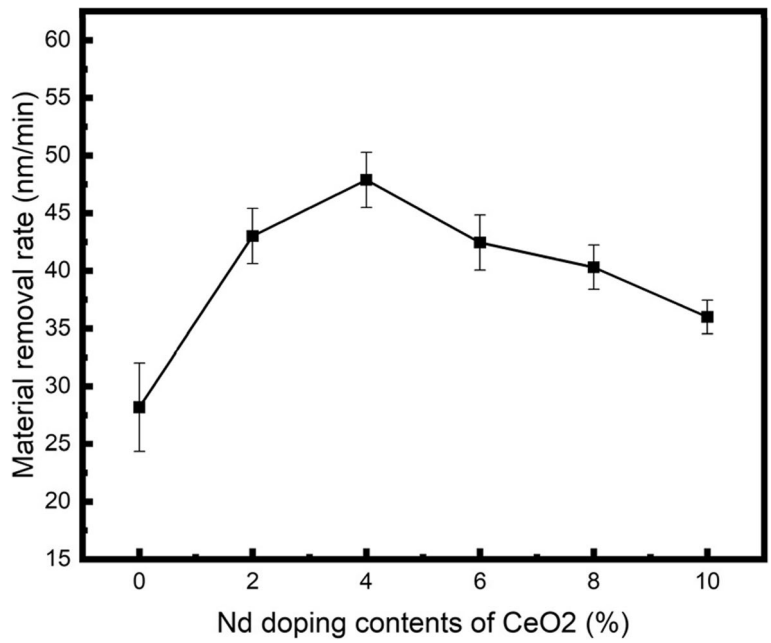


**Fig. 9** Curve of material removal rate with doping amount

The octahedral particles, with sharper edges compared to the polyhedral shape, generate higher localized pressure on the substrate when subjected to the same external force. This increased pressure facilitates the detachment of $SiO_2$ fragments from the substrate surface. Although the reduction in particle size due to doping leads to a decrease in the mechanical action and the depth of particle penetration into the substrate, the overall material removal rate is highest at a doping amount of 4%. However, when the doping amount exceeds 4%, the $Ce^{3+}$ concentration of the particles begins to decrease, leading to a reduction in chemical action. Although the abrasives have stabilized into an octahedral shape with good mechanical effect, the abrasive size is reduced, causing

some abrasives to become embedded in the polishing pad, thereby diminishing their effective polishing capability. Especially When doping reaches 8% or 10%, although the $Ce^{3+}$ concentration of the abrasive is higher than at 2%, the MRR decreases. This is due to the reduced particle size, which weakens the bonding between the abrasive particles and $SiO_2$ and diminishes mechanical action, leading to a lower MRR.

### 3.6 Surface quality analysis of polished and unpolished glass substrates

Surface roughness is a key factor influencing both the functional performance and the overall quality of a glass substrate. For instance, in applications involving optical devices, lenses, or optical systems, surface roughness contributes to light scattering, diffuse reflection, and optical distortion, consequently diminishing transparency, imaging precision, and overall optical performance [4]. Hence, within the CMP process, precise assessment and meticulous management of surface roughness stand as indispensable measures to uphold product excellence, ensure device reliability, and maintain process stability. Figure 10. illustrates the surface profile of the unpolished and polished glass substrate with $CeO_2$ and $Ce_{1-x}Nd_xO_2$. Compared to the high roughness of the unpolished glass substrate (Sa = 3.12 nm), the glass surfaces polished with $CeO_2$ and $Ce_{1-x}Nd_xO_2$ slurries appear smoother and free of noticeable bumps. Figure 11 highlights the surface roughness of glass substrates polished with different abrasives, showing that $Ce_{1-x}Nd_xO_2$ achieves lower roughness than $CeO_2$. Notably, the glass substrate polished with $Ce_{0.92}Nd_{0.08}O_2$ has the lowest roughness (Sa = 1.38 nm).

Based on these findings, several observations have emerged. First of all, the glass substrates polished by polishing slurries prepared by $Ce_{0.92}Nd_{0.08}O_2$ abrasive

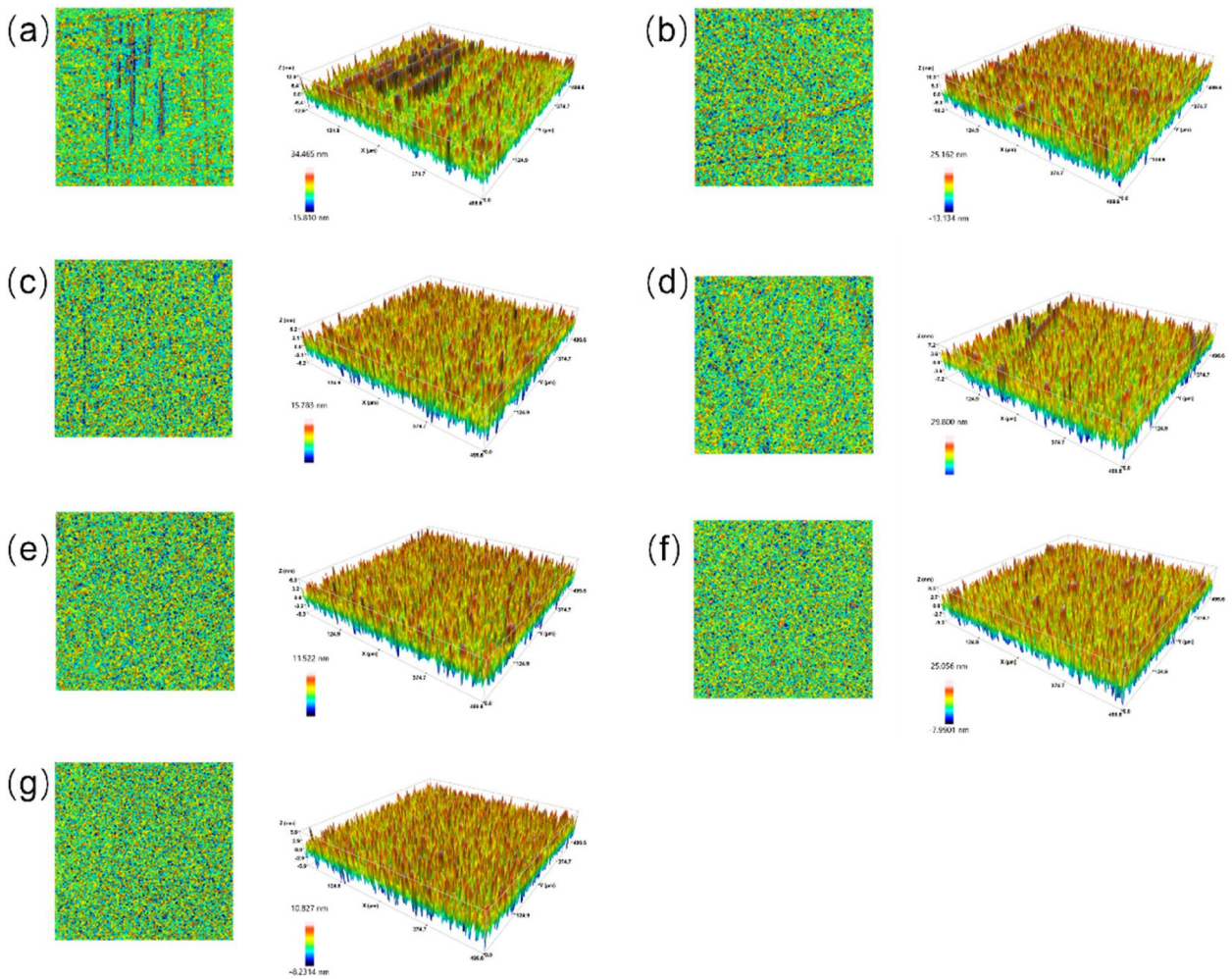


**Fig. 10** Surface profiles of glass substrates: (**a**) unpolished, Sa = 3.12 nm; (**b**-**g**) polished by $CeO_2$ and $Ce_{1-x}Nd_xO_2$: Sa = (2.71 nm;1.65 nm;1.83 nm; 1.68 nm; 1.38 nm; 1.56 nm

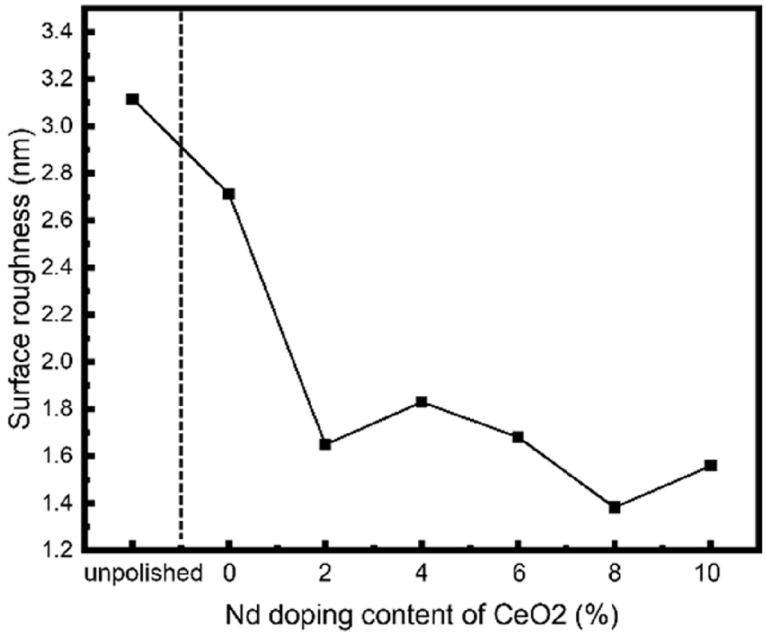


**Fig. 11** Surface roughness vs. different $Nd^{3+}$ doping contents

has the lowest surface roughness. However, according to previous experiments, the $Ce^{3+}$ concentration of $Ce_{0.92}Nd_{0.08}O_2$ abrasive is not the highest, nor is the abrasive size the largest. This suggests that while the chemical and mechanical effects of $Ce_{0.92}Nd_{0.08}O_2$ abrasive may not be the strongest, it still achieves the lowest surface roughness. This can be attributed to a balanced synergy between chemical bonding with $SiO_2$ and mechanical grinding, optimizing the polishing effect. When the doping amount is increased to 8%, the particle size of cerium oxide is reduced to 303 nm, resulting in a diminished mechanical effect. At this doping level, the $Ce^{3+}$ content on the surface is 34.63%, and the chemical bonding is less pronounced. During the polishing process, the cerium oxide abrasive particles predominantly bond to the rough peaks and are then removed via mechanical action. Due to the smaller particle size, the wear particles are less likely to scratch the substrate during the mechanical removal process. As a result, the rough peaks are effectively removed without causing scratches on the flat areas, leading to the lowest surface roughness observed.

When the doping amount is 4%, the $Ce_{0.96}Nd_{0.04}O_2$ abrasive exhibits the highest surface $Ce^{3+}$ concentration, indicating the strongest chemical activity. However, glass substrates polished with polishing slurries prepared by $Ce_{0.96}Nd_{0.04}O_2$ abrasive show the highest surface roughness. This is primarily due to two factors. First, the strong chemical interaction between the abrasive and $SiO_2$ leads to a strong bond, causing residual $Ce_{0.96}Nd_{0.04}O_2$ on the substrate surface. This adhesive effect results in the abrasive particles sticking to the substrate material, which increases surface roughness. Second, the increase in $Ce^{3+}$ content facilitates the bonding and removal of both rough peaks and flat areas. The removal of flat regions leads to the formation of grooves, further increasing the surface roughness. Additionally, although the particle size of the wear particles decreases to approximately 400 nm, reducing the mechanical action, the particles exhibit an octahedral morphology, which enhances the mechanical effect due to sharper edges and angles that generate higher local pressure. This allows for more effective removal of rough peaks. However, the combination of abrasive particle adhesion and over-polishing leads to an overall increase in surface roughness. For $CeO_2$ abrasive, although its morphology is a polyhedron, which is the least likely to cause surface scratches among the abrasive particles in this series, the amount of $SiO_2$ bonding is too small to effectively remove $SiO_2$ debris from the glass substrate. In this case, mechanical action outweighs chemical action, leading to inefficient removal of the rough peaks and consequently high surface roughness after polishing.

### 3.7 CMP mechanism analysis

From a microscopic perspective, as shown in Fig. 12(a) and (b), $Nd^{3+}$ doping leads to the reduction of $Ce^{4+}$ of $CeO_2$ abrasive. To balance the electrical and stress effects of doping [30], some $Ce^{4+}$ is converted into $Ce^{3+}$, forming oxygen vacancies [31]. Consequently, the $Ce^{3+}$ concentration and oxygen vacancy content on the

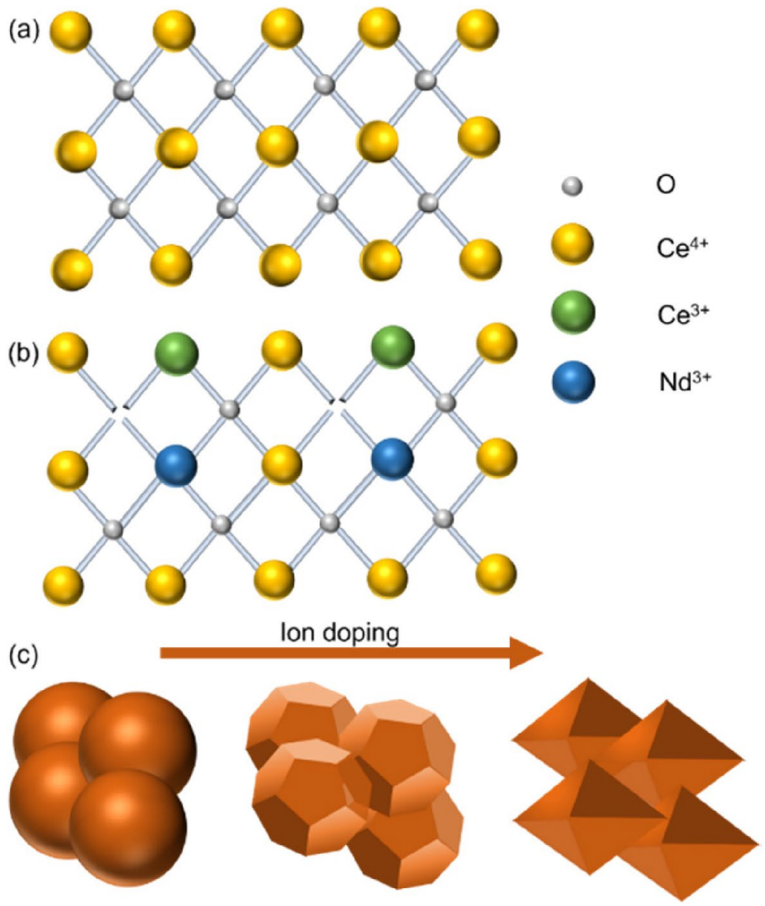


**Fig. 12** **a** Atomic structure of pure $CeO_2$ and (**b**) Nd-doped $CeO_2$ surfaces and (**c**) the shape changes of abrasive particles caused by doping

$Ce_{1-x}Nd_xO_2$ abrasives surface increase. On a larger scale, as shown in Fig. 12(c), $Nd^{3+}$ doping causes the abrasives to transition from a polyhedral to an octahedral shape and reduces their size. This alteration changes both the interaction pattern and the contact frequency during polishing.

Figure 13 illustrates a schematic of the mechanism of CMP for a glass substrate using $CeO_2$ abrasive. Abrasives are dispersed within the polishing pad and come into contact with the glass substrate, performing both chemical and mechanical roles [32]. Specifically, the chemical action involves the bonding between the Si–O—site of the glass substrate, post-water corrosion, and the Ce-OH on the $CeO_2$ surface, as represented by Eq. (7). Simultaneously, under the mechanical action exerted by polishing pads and abrasive particles, Si–O-Si bonds with relatively weak bonding strength are more likely to break, allowing $SiO_2$ debris to be taken away [33].

$$Ce - OH + SiO^{-} \rightarrow Ce - O - Si + OH^{-} \quad (7)$$

$Ce^{3+}$ of $CeO_2$ enhances the chemical interaction between $CeO_2$ and $SiO_2$ [18, 21, 31], leading to increased formation of Ce–O-Si bonds forming, which facilitates the removal of more $SiO_2$ fragments and thereby improves the MRR during polishing. The mechanical aspect involves the abrasive particles grinding the softened layer. As shown in Fig. 13, the abrasive particles, driven by the polishing pad, grind the rough peaks on the softened glass surface to achieve smoothness. However, due to the unique groove structure of the polishing pad, some smaller abrasives are trapped in the grooves and cannot make contact with the glass substrate surface, rendering them ineffective. Additionally, the effective area of direct contact between larger abrasive and the glass substrate surface increases, and the larger abrasives exert a greater local load on the substrate, typically resulting in lower polishing quality [34]. When the abrasive particles are polyhedral, the grinding mode is rolling, whereas with octahedral particles, the grinding mode is sliding. This sliding mode creates greater local pressure, making material removal easier but also increasing the risk of surface scratching [35].Therefore, when either the chemical or mechanical effects are too strong, the Sa increases.

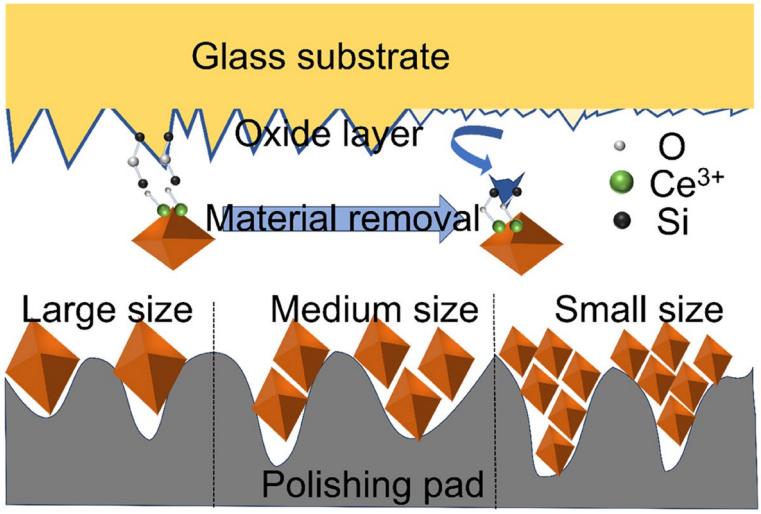


**Fig. 13** CMP mechanism diagram

Only when the two effects are balanced and optimally coordinated will the Sa reach its lowest point.

## 4 Conclusion

1. $Nd^{3+}$-doped cerium oxide was successfully synthesized using the salt melting method. The doped cerium oxide exhibits higher surface $Ce^{3+}$ content and smaller particle size. Additionally, the morphology transitions from polyhedral to octahedral.
2. The $Ce^{3+}$ concentration on the surface of cerium oxide initially increases and then decreases with increasing $Nd^{3+}$ content. The increase in $Ce^{3+}$ content reduces the contact angle of the polishing slurry, enhancing the effective contact between the abrasive particles and the substrate. This leads to improvements in both the chemical and mechanical effects during the polishing process.
3. With the increase in $Nd^{3+}$ doping, the particle size of cerium oxide decreases, which leads to a reduction in the mechanical effect due to the smaller particle size.
4. $Nd^{3+}$ doping causes the cerium oxide morphology to shift from polyhedral to octahedral. The octahedral shape, with its sharper edges and angles, generates higher local pressure during polishing, which increases the friction coefficient and enhances the mechanical action in the polishing process.
5. At an 8% doping level, a balance between chemical and mechanical effects is achieved, resulting in the lowest surface roughness.

## Supplementary Information

The online version contains supplementary material available at https://doi.org/10.1007/s44251-025-00072-x.

Supplementary Material 1.

**Acknowledgements**
This work was supported by the National Natural Science Foundation of China (Grant Number 52475204), Science and Technology Major Project of Inner Mongolia Autonomous Region in China (No. 2021ZD0028), and Shanghai Engineering Research Center for Integrated Circuits and Advanced Display Materials, Shanghai University, Shanghai200444, China.

**Authors' contributions**
CRediT authorship contribution statement. Yesheng Zhang: Writing – original draft, Project administration, Methodology, Investigation. Hong Lei: Writing – review & editing. Liqiang Luo: Formal Analysis, Supervision. Jianhua Zhang: Formal Analysis, Supervision.

**Data availability**
Data available on request from the authors.

## Declarations

**Competing interests**
No conflict of interest exits in the submission of this manuscript, and the manuscript is approved for publication by all the authors concerned. I would like to declare on behalf of my co-authors that the work described is original research that has not been published previously, and is not currently under consideration for publication elsewhere, in whole or in part. All the authors listed have approved the manuscript that is enclosed.

Received: 8 October 2024 Revised: 29 December 2024 Accepted: 6 February 2025
Published online: 18 February 2025

**References**

1. Zhang L, Wang S, Wang T, Lu X (2023) Roles of phthalic acid and oleic acid on chemical mechanical polishing in alkaline slurries for cobalt

interconnects. ECS J Solid State Sci Technol 12(7):074007. https://doi.org/10.1149/2162-8777/ace796
2. Teng Q, Hu Y, Cheng R, Wu Y, Zhou G, Gao D (2023) Reliability challenges in CMOS technology: a manufacturing process perspective. Microelectron Eng 281:112086. https://doi.org/10.1016/j.mee.2023.112086
3. Zhang L, Wang S, Wang T, Lu X (2023) Polishing mechanisms of various surfactants in chemical mechanical polishing relevant to cobalt interconnects. Int J Adv Manuf Technol 128(11–12):5425–5436. https://doi.org/10.1007/s00170-023-12246-8
4. Yadav HNS, Das M (2024) Advances in finishing of optical complex substrates: a comprehensive review. Opt Laser Technol 176:110938. https://doi.org/10.1016/j.optlastec.2024.110938
5. Wang W, Lu X, Wu X, Zhang Y, Wang R, Yang D, Pi X (2023) Chemical-mechanical polishing of 4H silicon carbide wafers. Adv Mater Interfaces 10(13):2202369. https://doi.org/10.1002/admi.202202369
6. Wang D, Liu L, Zhang Z, Peng Q, Shi C, Liu X, Liu X, Zhou H, Wen W (2024) Atomic-scale planarization surface of quartz glass induced by novel green chemical mechanical polishing using three ingredients. Mater Today Sustain 25:100669. https://doi.org/10.1016/j.mtsust.2024.100669
7. Tao H, Zeng Q, Liu Y, Zhao D, Lu X (2023) Effects of grinding-induced surface topography on the material removal mechanism of silicon chemical mechanical polishing. Appl Surf Sci 631:157509. https://doi.org/10.1016/j.apsusc.2023.157509
8. Chen Y, Zhong L, Chen A, Fu M, Lu X (2023) Highly dispersed Gd-CeO2 nanocrystals supported on mesoporous silica composite particles towards photochemical (Photo-Assisted Chemical) mechanical polishing. Ceram Int 49(11):16932–16943. https://doi.org/10.1016/j.ceramint.2023.02.055
9. Brugnoli L, Miyatani K, Akaji M, Urata S, Pedone A (2023) New Atomistic Insights on the chemical mechanical polishing of silica glass with ceria nanoparticles. Langmuir 39(15):5527–5541. https://doi.org/10.1021/acs.langmuir.3c00304
10. Wang L, Ren G, Xie W, Zhang J, Pan D, Wang S (2024) Simple and facile synthesis of single-crystal CeO2 Abrasives and its highly efficient removal mechanism on SiO2 film. Appl Surf Sci 654:159510. https://doi.org/10.1016/j.apsusc.2024.159510
11. Sabia R, Stevens HJ (2000) Performance characterization of cerium oxide abrasives for chemical-mechanical polishing of glass. Mach Sci Technol 4(2):235–251. https://doi.org/10.1080/10940340008945708
12. Seo J, Gowda A, Babu SV (2018) Almost complete removal of ceria particles down to 10 Nm size from silicon dioxide surfaces. ECS J Solid State Sci Technol 7(5):P243–P252. https://doi.org/10.1149/2.0131805jss
13. Schmitt R, Nenning A, Kraynis O, Korobko R, Frenkel AI, Lubomirsky I, Haile SM, Rupp JLM (2020) A review of defect structure and chemistry in ceria and its solid solutions. Chem Soc Rev 49(2):554–592. https://doi.org/10.1039/C9CS00588A
14. Paier J, Penschke C, Sauer J (2013) Oxygen defects and surface chemistry of ceria: quantum chemical studies compared to experiment. Chem Rev 113(6):3949–3985. https://doi.org/10.1021/cr3004949
15. Cheng J, Huang S, Li Y, Wang T, Xie L, Lu X (2020) RE (La, Nd and Yb) doped CeO2 abrasive particles for chemical mechanical polishing of dielectric materials: experimental and computational analysis. Appl Surf Sci 506:144668. https://doi.org/10.1016/j.apsusc.2019.144668
16. Kim E, Lee J, Bae C, Seok H, Kim H-U, Kim T (2022) Effects of trivalent lanthanide (La and Nd) doped ceria abrasives on chemical mechanical polishing. Powder Technol 397:117025. https://doi.org/10.1016/j.powtec.2021.11.069
17. Xia X, Lan Y, Li J, Chen C, Xu B, Luo X, Mao X (2020) Facile synthesis of nanoceria by a molten hydroxide method and its photocatalytic properties. J Rare Earths 38(9):951–960. https://doi.org/10.1016/j.jre.2019.11.007
18. Ma J, Xu N, Hu J, Luo Y, Lin Y, Pu Y (2023) Doping strategy on properties and chemical mechanical polishing performance of CeO2 abrasives: a DFT assisted experimental study. Appl Surf Sci 623:156997. https://doi.org/10.1016/j.apsusc.2023.156997
19. Xu N, Luo Y, Ma J, Lin Y, Zhu X, Pu Y (2024) Enhancement mechanism of Y-Doped Ce1−xYxO2 for photocatalytic-assisted chemical-mechanical polishing. Mater Today Commun 38:107791. https://doi.org/10.1016/j.mtcomm.2023.107791
20. Yuan X, Chen C, Lei H, Zhang Z (2023) Synthesis, characterization of CeO2@ZIF-8 composite abrasives and their chemical mechanical polishing behavior on glass substrate. Ceram Int 49(3):5189–5198. https://doi.org/10.1016/j.ceramint.2022.10.037
21. Fan Y, Jiao J, Zhao L, Tang J, Chen C, Fan N (2024) Nd-doped porous CeO2 abrasives for chemical mechanical polishing of SiO2 films. Mater Sci Semicond Process 175:108265. https://doi.org/10.1016/j.mssp.2024.108265
22. Wu Z, Shen J, Wu X, Peng Y, Lin S, Huang L, Huang X, Zhu L (2023) Effect of dispersion performance of polishing slurry on the polishing quality of glass-ceramics in bonnet polishing. Int J Adv Manuf Technol 127(1–2):107–121. https://doi.org/10.1007/s00170-023-11532-9
23. Zhang W, Lei H, Liu W, Zhang Z, Chen Y, Hu X, Ye X (2024) Effect of EDTA-modified alumina composite abrasive on the CMP performance of sapphire substrate. Mater Chem Phys 312:128651. https://doi.org/10.1016/j.matchemphys.2023.128651
24. Ma J, Xu N, Luo Y, Liu Q, Pu Y (2023) Defect generation and morphology transformation mechanism of CeO2 particles prepared by molten salt method. Ceram Int 49(3):4929–4943. https://doi.org/10.1016/j.ceramint.2022.10.007
25. Wang T, Chen Y, Chen A, Chen Y (2022) Development of Carbon Sphere/Ceria (CS/CeO2) heterostructured particles and their applications to functional abrasives toward photochemical mechanical polishing. Appl Surf Sci 593:153449. https://doi.org/10.1016/j.apsusc.2022.153449
26. Pan J, Wang S, Chen A, Chen Y, Wang M, Chen Y (2022) Visible-Light-Active Mesoporous Ceria (CeO2) nanospheres for improved photocatalytic performance. J Alloys Compd 898:162895. https://doi.org/10.1016/j.jallcom.2021.162895
27. Ye W, Baoguo Z, Pengfei W, Min L, Dexing C, Wenhao X (2023) Improving the dispersion stability and chemical mechanical polishing performance of $CeO_2$ slurries. ECS J Solid State Sci Technol 12(4):044004. https://doi.org/10.1149/2162-8777/accaa5
28. Zhong Z-W (2020) Recent developments and applications of chemical mechanical polishing. Int J Adv Manuf Technol 109(5–6):1419–1430. https://doi.org/10.1007/s00170-020-05740-w
29. Banerjee G, Rhoades RL (2008) Chemical mechanical planarization historical review and future direction. ECS Trans 13(4):1–19. https://doi.org/10.1149/1.2912973
30. Li Z, Jin L, Cao Z, Zhang C, Cao X, Han G, Peng S, Liu Y (2023) Development and characterization of a novel RE3+ doped core-shell CeO2 abrasive system and its glass CMP investigations. Appl Surf Sci 638:158055. https://doi.org/10.1016/j.apsusc.2023.158055
31. Ma J, Xu N, Luo Y, Lin Y, Pu Y (2023) Enhancing the polishing efficiency of $CeO_2$ abrasives on the $SiO_2$ substrates by improving the $Ce^{3+}$ concentration on their surface. ACS Appl Electron Mater 5(1):526–536. https://doi.org/10.1021/acsaelm.2c01553
32. Matijević E, Babu SV (2008) Colloid aspects of chemical-mechanical planarization. J Colloid Interface Sci 320(1):219–237. https://doi.org/10.1016/j.jcis.2007.11.057
33. Hoshino, T.; Kurata, Y.; Terasaki, Y.; Susa, K. Mechanism of Polishing of SiO2 Films by CeO2 Particles.
34. Oh M-H, Singh RK, Gupta S, Cho S-B (2010) Polishing behaviors of single crystalline ceria abrasives on silicon dioxide and silicon nitride CMP. Microelectron Eng 87(12):2633–2637. https://doi.org/10.1016/j.mee.2010.07.040
35. Hu P, Chen Y, Sun R, Chen Y, Yin Y, Wang Z (2017) Synthesis, characterization and frictional wear behavior of ceria hybrid architectures with 111 exposure planes. Appl Surf Sci 401:100–105. https://doi.org/10.1016/j.apsusc.2017.01.005

## Publisher's Note